



POLITECNICO DI TORINO
Repository ISTITUZIONALE

Efficiency of closed loop geothermal heat pumps: A sensitivity analysis

Original

Efficiency of closed loop geothermal heat pumps: A sensitivity analysis / Alessandro Casasso; Rajandrea Sethi. - In: RENEWABLE ENERGY. - ISSN 0960-1481. - ELETTRONICO. - 62(2014), pp. 737-746.

Availability:

This version is available at: 11583/2514912 since:

Publisher:

Elsevier

Published

DOI:10.1016/j.renene.2013.08.019

Terms of use:

openAccess

This article is made available under terms and conditions as specified in the corresponding bibliographic description in the repository

Publisher copyright

(Article begins on next page)

1

2

3 Efficiency of closed loop geothermal heat pumps: a
4 sensitivity analysis

5

6 *Alessandro Casasso, Rajandrea Sethi**

7 DIATI – Dipartimento di Ingegneria dell’Ambiente, del Territorio e delle Infrastrutture

8 Politecnico di Torino, Corso Duca degli Abruzzi 24, 10129, Turin, Italy

9 *Corresponding author (email: rajandrea.sethi@polito.it)

10 **Abstract**

11 Geothermal heat pumps are becoming more and more popular as the price of fossil fuels is
12 increasing and a strong reduction of anthropogenic CO₂ emissions is needed. The energy
13 performances of these plants are closely related to the thermal and hydrogeological properties of the
14 soil, but a proper design and installation also plays a crucial role. A set of flow and heat transport
15 simulations has been run to evaluate the impact of different parameters on the operation of a GHSP.
16 It is demonstrated that the BHE length is the most influential factor, that the heat carrier fluid also
17 plays a fundamental role, and that further improvements can be obtained by using pipe spacers and
18 highly conductive grouts. On the other hand, if the physical properties of the soil are not surveyed
19 properly, they represent a strong factor of uncertainty when modelling the operation of these plants.
20 The thermal conductivity of the soil has a prevailing importance and should be determined with in-
21 situ tests (TRT), rather than assigning values from literature. When groundwater flow is present, the
22 advection should also be considered, due to its positive effect on the performances of BHEs; by
23 contrast, as little is currently known about thermal dispersion, relying on this transport mechanism
24 can lead to an excessively optimistic design.

25

26 **Keywords:**

27 Low-enthalpy geothermal energy, Borehole Heat Exchanger, Ground Source Heat Pump, Heat
28 transport, Groundwater

29 **1. Introduction**

30 Ground Source Heat Pumps (GSHP) are space heating and cooling plants which exploit the soil as a
31 thermal source or sink, through the circulation of a heat carrier fluid in a closed pipe loop. Different
32 pipe arrangements are available, among which the most common is the Borehole Heat Exchanger, a
33 vertical pipe loop reaching depths of 50 to 200 m (Fig.1). Below a depth of a few meters from the
34 ground surface, the seasonal variation of the air temperature disappears due to the large thermal
35 inertia of the soil. Therefore, if compared to the air, the soil is a warmer source for heating during
36 winter and a cooler sink for cooling during summer, and higher system efficiencies can therefore be
37 achieved compared to Air Source Heat Pumps.

38 GSHPs are rapidly spreading in Europe, China and USA, and have a great potential for energy, cost
39 and CO₂ emission saving [1]. About 100,000 low-enthalpy geothermal plants are installed every
40 year in Europe, mainly for new dwellings in Sweden, Germany and France [2, 3]. According to
41 Saner et al. [4], the use of GSHP in place of methane furnaces allows the CO₂ emissions to be
42 reduced by up to 84%, depending on the sources used for the production of electricity. From the
43 economic point of view, the geothermal heat pumps lead to a considerable reduction of the
44 maintenance costs and, although their installation is more expensive than the other heating and
45 cooling plants, the payback periods proved to be reasonable, i.e. less than 10 years [5-7].

46 Since the thermal exploitation of the soil induces a gradual temperature drift, an accurate heat
47 transport modelling of soil and aquifer systems is essential for a correct design of GSHPs. Indeed,
48 the efficiency of the heat pump is strongly influenced by the temperature of the heat carrier fluid,
49 which in turns depends on the temperature of the surrounding soil. To estimate the thermal impact
50 of BHEs and the working temperatures of the heat carrier fluid, different methods have been
51 developed, which can be divided into analytical, semi-analytical and numerical.

52 The Kelvin infinite line source [8] and the infinite cylindrical source [9] are the simplest analytical
53 methods for estimating the thermal disturbance induced by a BHE, since they rely on the

54 assumption of a purely conductive and radial heat transport. Their main limitation is that of not
55 accounting for the vertical thermal gradient and fluxes [10] and for the heterogeneity of the heat
56 exchange over the length. Moreover, the advective and dispersive heat transport occurring in
57 aquifer systems is also neglected. Nevertheless, these analytical solutions are still widely used for
58 the interpretation of Thermal Response Tests [11], since they last for a short time (48÷72 h) and
59 therefore the vertical heat transport can be neglected. The subsurface flow and the seasonal changes
60 of groundwater levels can significantly alter the results of a TRT, as pointed out by Bozdağ et al.
61 [12]. To overcome this problem, Wagner et al. [13] recently developed a method for the
62 interpretation of TRTs in the presence of strong groundwater flow.

63 The semi-analytical method proposed by Eskilson [14] takes into account the finite length of the
64 exchanger and different BHE field layouts, but the advection and the dispersion are neglected. This
65 method is applied by two of the most popular BHE design software programmes, Earth Energy
66 Design [15] and GLHEPRO [16].

67 Analytical models which take into account the beneficial effects of groundwater flow [17], of the
68 finite length of the BHE [18], and both them together [19] have been developed in the last few
69 years, and they could be used in the future for the dimensioning of BHE fields.

70 Recently, numerical modelling has often been applied to the design of BHE fields. The finite-
71 difference modelling software MODFLOW can be used coupled with the solute transport package
72 MT3D (or MT3DMS) and by applying the analogy between heat and solute transport [20, 21], or
73 with the specific heat transport package SEAWAT [22]. On the other hand, the finite element
74 software FEFLOW includes a special package for the simulation of BHEs [23, 24] which is
75 particularly suitable for non conventional BHE field layouts and for taking into account the thermal
76 advection and dispersion in aquifer systems.

77

78 The heat transport simulation of GSHPs permits the assessment of their performances, which are
79 influenced by the properties of the exchanger and the thermo-hydrogeological parameters of the

80 soil. According to Chiasson et al. [25], groundwater flow significantly enhances the performances
81 of BHEs, and the Peclet number is a good indicator for whether advective transport needs to be
82 taken into account or neglected. Wang et al. [26] have developed a method to estimate the velocity
83 of groundwater movement measuring the temperature profiles in a BHE. Lee [27] has investigated
84 the effect of vertical heterogeneities of the soil thermal conductivity, concluding that the adoption
85 of depth-averaged thermal parameters is appropriate. Chung and Choi [28] have found that an
86 increase of the fluid flow rate reduces the heat transfer rate per unit length. Delaleux et al. [29] have
87 studied the increase of the thermal conductivity of grouts with the addition of graphite flakes,
88 concluding that a noticeable heat transfer improvement is achieved by BHEs. Jun et al. [30] have
89 evaluated the influence of running time, pipe spacing, grout conductivity, borehole depth, fluid flow
90 rate, inlet fluid temperature and soil type on the heat transfer length and on the thermal resistance of
91 borehole and soil. Michouopoulos and Kiriakis [31] have found a non-linear relation between the
92 BHE length and the heat pump consumption, which can be used for optimization processes in the
93 dimensioning of large plants. The aforementioned studies deal with single or few parameters, but a
94 thorough comparative analysis of all these factors together is still missing, and constitutes the
95 objective of this work. The functioning of a single BHE was simulated for 30 years, using a
96 benchmark cyclic thermal load and changing the operational parameters of the scenario. The
97 resulting fluid temperatures at the end of the BHE were processed and used to estimate the COP of
98 the heat pump and its annual energy consumption under different conditions. On the basis of the
99 results it is possible to draw some practical conclusions on the margins of improvement of BHEs
100 and on the proper choice of soil parameters for the simulations.

101

102 **2. The modelling framework**

103 The sensitivity analysis has been carried out on the design parameters of the BHE (geometrical
104 setting, properties of the materials, flow rate etc.) and on the physical properties of the soil and the

105 aquifer (thermal conductivity, groundwater flow velocity etc.), with the aim of evaluating their
 106 relative impact on the performances of a GSHP (i.e. evolution of the heat carrier fluid temperatures,
 107 energy consumption of the heat pump) in a realistic scenario and in long-term perspective.

108 The case study involves the simulations of the heating system of a house in the North of Italy, with
 109 a heated surface of 150 m² and a good thermal insulation. A geothermal heat pump connected to a
 110 BHE with a single U-pipe configuration is used only for heating. A cyclic thermal load (see Fig.2)
 111 has been set , with a total heat abstraction of 12 MWh per year (80 kWh m⁻²y⁻¹), which is equivalent
 112 to the energy produced by 1200 m³ of methane or 1250 l of gasoil using an efficient condensation
 113 boiler. The simulations last for 30 years, which is a sufficiently long time span to assess the long-
 114 term sustainability of the thermal exploitation of the soil.

115

116 The simulation of the heat exchange of the BHE with the soil and the aquifer system has been
 117 performed with FEFLOW 6.0, a 3D finite element flow and solute/heat transport model [32, 33]
 118 that includes specific tools for the simulation of Borehole Heat Exchangers [23, 24]. The software
 119 solves the coupled equations of flow and heat transport in the soil, and the BHE is modelled as an
 120 internal boundary condition of the 4th kind (thermal well).

121 The heat transport occurs by conduction (driven by thermal gradients), advection (due to the
 122 groundwater flow) and dispersion (due to deviations from the average advective velocity), which
 123 are described by the heat conservation equation in the porous medium:

$$124 \quad \frac{\partial}{\partial t} [(\varepsilon \rho_w c_w + (1 - \varepsilon) \rho_s c_s) T] + \frac{\partial}{\partial x_i} (\rho_w c_w q_i T) + \frac{\partial}{\partial x_i} \left[(\lambda_{ij}^{cond} + \lambda_{ij}^{disp}) \frac{\partial T}{\partial x_j} \right] = H$$

125

1

126 where ε is the porosity, ρ_s and ρ_w are the density of the solid and liquid phase, c_s and c_w are the
 127 specific heat of the solid and liquid phase, T is the temperature (which has been assumed equal for

128 both the phases), x_i is the i-th axis (i.e. $x_1 \equiv x, x_2 \equiv y, x_3 \equiv z$) and q_i is the i-th component of the
 129 Darcy velocity (i.e. relative to the i-th axis), and H is the heat source or sink (the BHE in this case),
 130 The first term of Eq.1 describes the soil temperature variation with time, involving the porosity ε
 131 and the heat capacity of the solid matrix $(\rho c)_s$ and of water $(\rho c)_w$.

132 The second term describes the advection, which depends on the Darcy velocity q .

133 The conduction and dispersion are respectively described by the tensors of the thermal conductivity
 134 λ_{ij}^{cond} and λ_{ij}^{disp} (third term of Eq.1):

$$135 \quad \lambda_{ij}^{cond} = \begin{cases} (1-\varepsilon)\lambda_s + \varepsilon\lambda_w & \text{for } i = j \\ 0 & \text{for } i \neq j \end{cases}$$

136 2

$$137 \quad \lambda_{ij}^{disp} = \rho_w c_w \left[\alpha_T q \delta_{ij} + (\alpha_L - \alpha_T) \frac{q_i q_j}{q} \right]$$

138 3

139 where λ_s and λ_w are the thermal conductivities of the solid matrix and of groundwater, α_L and α_T
 140 are the longitudinal and the transverse dispersivity (with respect to the direction of groundwater
 141 flow) and q is the modulus of the Darcy velocity.

142
 143 The temperature of the soil at the borehole wall, calculated by the 3D finite-element modelling
 144 code, is used to solve the balance of the thermal fluxes inside the BHE according to the Thermal
 145 Resistance and Capacity Model (TRCM) of Bauer et al. [34]. The BHE is decomposed into
 146 different elements (inlet and outlet pipe, grout zones, borehole wall), which are represented by the
 147 nodes of the circuit, connected by thermal resistances, which depend on the geometrical settings and
 148 the physical properties of the materials. Thermal energy conservation equations are solved, which
 149 describe the balance of thermal fluxes between the components of the BHE, and the temperature of
 150 each component is calculated [23]. Since no abrupt changes occur in the thermal load, the analytical

151 method based on Eskilson and Claesson's solution [35], which considers a stationary equilibrium
152 between the soil and the BHE, has been used in the simulations in order to reduce the computational
153 time if compared to the Al Khoury et al.'s [36, 37] transient model.

154

155 A very large square mesh domain, with a side of 1000 m and a thickness of 150m, has been used to
156 avoid boundary effects on the computed BHE fluid temperatures. The 31 flat slices are equally
157 spaced (5m of distance) and the total number of nodes is 15531. The mesh density has been set
158 using the "BHE node rule" [38], positioning the nodes around the BHE on the vertexes of a regular
159 hexagon, with a radius of 0.46 m (6.13 times the borehole radius), since Diersch et al. [24] proved
160 that this mesh density achieves a higher precision in the results, even when compared with finer
161 meshes.

162

163 The thermal balance of the soil around the BHE has been reproduced choosing appropriate
164 boundary conditions. The temperature of the soil is almost constant through the year and, at an
165 infinite distance from the BHE, it is not affected by the thermal exchange. Constant temperature
166 values (1st kind heat transport b.c.) have therefore been imposed at the lateral boundaries of the
167 domain, at least 500 m far away from the BHE. The heat flux coming from the deep layers of the
168 Earth (geothermal flux), which has a mean value of 0.065 Wm^{-2} on the continental crust [39],
169 induces a temperature vertical gradient with typical values around $0.03 \text{ }^{\circ}\text{C/m}$. According to these
170 considerations, a temperature of 12°C has been set at the border or the first slice (which is a typical
171 value of the annual mean air temperature in Northern Italy), incrementing the temperatures of
172 0.15°C every 5m of depth ($0.03 \text{ }^{\circ}\text{C/m}$). The initial conditions have been set consistently with the
173 boundary conditions, with a homogeneous distribution of the soil temperature at each slice.

174

175 An unconfined aquifer, with a water table depth of 20m in the centre of the mesh (where the BHE is
176 positioned), has been modelled assigning constant hydraulic head (1st kind) flow boundary

177 conditions along the mesh borders. A homogeneous and isotropic hydraulic conductivity
178 ($K = 10^{-4} \text{ m/s}$) has been assigned, and different hydraulic gradients, ranging between 1‰ and 20‰,
179 have been imposed to change the groundwater flow velocity. Also different values of the saturated
180 thickness of the phreatic aquifer have been adopted, ranging from 10m to 50m in the middle of the
181 mesh, where the BHE is located.

182

183 A large set of simulations has been run in order to ascertain the influence of design parameters
184 (length, pipe spacing, pipe diameter, heat carrier fluid and its flow rate, grout thermal conductivity),
185 soil thermal (thermal conductivity of the solid matrix, thermal dispersivity) and hydrogeological
186 properties (groundwater flow velocity, aquifer saturated thickness) on the performances of a BHE
187 over a long operation period (30 years).

188 The adopted values of the BHE length range between 50 and 100 m, using a default value of 75 m.
189 The borehole diameter is 0.15 m for all the simulations, and the HDPE pipes have an external
190 diameter of 32mm and a wall thickness of 2.9 mm. The pipe spacing depends on the kind of spacers
191 and from the pipe curvature given by the coil shape, which they keep even when they are unrolled:
192 it varies therefore with depth and could not be known precisely. Different values have therefore
193 been adopted, ranging from 35 to 117 mm between the pipe centres.

194 A set of simulation has been run to assess the performances of the most commonly adopted heat
195 carrier fluids, and also different flow rates have been assigned ($0.1 \div 0.7 \text{ ls}^{-1}$ with propylene glycol at
196 25% weight concentration). The default fluid is calcium chloride at 20% weight, which proved to be
197 the most performing one.

198 The thermal conductivity of the BHE filling can vary in a wide range, and values between 1 and 5
199 $\text{Wm}^{-1}\text{K}^{-1}$ have therefore been adopted, while its thermal capacity does not experience great
200 variations, and hence a unique value ($2 \text{ MJm}^{-3}\text{K}^{-1}$) has been used for all the simulations.

201 Some of the thermal and hydrogeological parameters of the soil have been kept constant for all the
202 simulations, like the thermal properties of water ($\lambda_w = 0.6 \text{ Wm}^{-1}\text{K}^{-1}$ and $(\rho c)_w = 4.2 \text{ MJm}^{-3}$), the
203 thermal capacity of the soil solid phase ($(\rho c)_s = 2.52 \text{ MJm}^{-3}$) and both the total and the effective
204 porosity (respectively $\varepsilon = 0.3$ and $n_e = 0.2$), while the others have been changed to assess their
205 influence on the performances of the geothermal systems. As the heat transport occurs by
206 conduction, advection and dispersion, large ranges of the solid phase thermal conductivity ($1 \div 3$
207 $\text{Wm}^{-1}\text{K}^{-1}$), the Darcy velocity of groundwater ($0 \div 17.32 \text{ md}^{-1}$) flow and the longitudinal/transverse
208 thermal dispersivity ($0 \div 5 \text{ m}$) have therefore been investigated.

209

210 The time series of the borehole fluid temperatures (Fig.3A) have been processed, calculating a
211 cumulative temperature distribution (Fig.3B) during the heating seasons over the whole simulation
212 period (30 years), which serves as a synthetic indicator to compare the different cases and to draw
213 conclusions on the energetic performance of the system. Observing the fluid temperature duration
214 curves in Fig.4 and Fig.5, one can understand how long will the heat pump work in a certain source
215 temperature range. For example, Fig.4A shows that, for a 75m long BHE, the mean fluid
216 temperature is below 0°C for the 19.51% of the heating period (say, 41.37 days a year), while this
217 percentage rises up to 50.86% for a 50m long borehole (107.83 days a year).

218

219 The Coefficient of Performance (COP), which is the ratio between the heating power delivered to
220 the building and the electrical power absorbed by the heat pump, depends on the temperatures of the
221 heat source (the BHE fluid) and of the heat sink (the heating terminals of the building). The
222 relationship of COP from fluid temperatures has been approximated with a linear formula:

223

$$COP = a + b \cdot T_f$$

224

4

225 where T_f is the average fluid temperature between the inlet and outlet pipes of the BHE, while a
226 and b depend on the heating terminal. For this study, we have set $a = 4$ and $b = 0.1 K^{-1}$, which are
227 typical values for radiant panels at 35°C.

228 The estimated COP values at each time step (COP_i) have been used to calculate the energy
229 consumption of the heat pump:

$$230 \quad HPC = \sum_{i=1}^n \frac{BHL_i}{COP_i} \cdot \Delta t$$

231 5

232 where BHL_i is the value of the BHE heat load at the i -th time step and Δt is the length of the
233 constant time step (1 day). The electricity consumed by the heat pump gradually increases, as the
234 soil and the BHE fluid is gradually cooling: the average value of yearly electricity consumption in
235 the operation period (30 years) has been therefore used to evaluate the energy performance of the
236 different BHE settings (Fig.6).

237

238 **3. Results and discussion**

239 The results of the long-term BHE simulations have been processed and compared in order to
240 understand which is the relative importance of each parameter on the performances of the system
241 and which is the margin of error due to the uncertainty in its determination, in particular for soil
242 properties. Statistics about the calculated fluid temperatures (average, RMSE), the Seasonal
243 Performance Factor (SPF) and the heat pump consumption for each simulation are summarized in
244 the tables reported in the supporting information.

245

246 The length of the Borehole Heat Exchanger(s) plays a crucial role in the design process, because it
247 accounts for about half of the total installation cost in single-house plants (see Blum et al. [40]).

248 Varying the BHE length between 50 and 100m, we observe a strong variation of the cumulate

249 distributions of the average fluid temperatures (Fig.4A) and of the value of the minimum fluid
250 temperature, which is a critical parameter in the operation of a GSHP. The effect of the length
251 increase is non-linear and diminishes for larger BHE sizes: for example, incrementing the length by
252 between 50 and 75 m results in an increment of 2.80°C in the mean temperature, and of 1.58°C
253 when the increment is from 75 m to 100 m; the minimum inlet temperatures are incremented
254 respectively by 4.15°C and 1.92°C in the same ranges. The differences in the distributions of fluid
255 temperatures also have a noticeable impact on the energy expense of the heat pump, as shown in
256 Fig.6A. As for the cumulate distributions of the fluid temperatures, the effect of additional BHE
257 length is reduced as the borehole depth increases (- 5.88% between 50 m and 75 m, -2.77% between
258 75 m and 100 m).

259

260 The improvement of the energy performance with longer exchangers is compensated by a rise in the
261 installation costs, which are the main drawback of geothermal heat pumps. In the dimensioning of
262 BHE fields, usually a minimum and/or maximum fluid temperature constraint is imposed, and the
263 minimum required borehole size is calculated [15, 16]. This approach minimizes the installation
264 costs, but the maintenance costs are not taken into account, and the extra-cost due to a low COP can
265 overcome the initial saving incurred with a smaller drilled depth. Starting from the results of the
266 sensitivity analysis on the length of the BHE, we have considered the typical electricity and BHE
267 installation costs of Italy (see Tab. 2) and calculated the total costs of installation and maintenance
268 of the GSHP over a lifetime of 30 years. Since the unit cost of electricity is likely to increase over
269 the next few decades, the analysis took into account different increase rates, in the range
270 between 0% and 5%. In Fig.7, the ratio between the lifetime cost for each BHE length and the most
271 expensive solution for each scenario of energy cost increase is shown, to identify the optimal size
272 for each case. We observe that higher increments of the unit cost of electricity enlarge the optimal
273 range of the BHE length, and shift it towards larger values; although it is not shown in the graph, a
274 decrease of the drilling cost also achieves the same effect. GSHPs need larger investments

275 compared to the other heating and cooling plants, and loan rates have been also considered when
276 evaluating the optimal length. Nevertheless, the influence of the interest rate on the total cost of the
277 plant over its lifetime proved to be negligible, compared to the cost of electricity and its increasing
278 trend.

279 A default length of 75 m was used in the other simulations, since it proved to be a reasonable choice
280 for most of the scenarios depicted in Fig.7. The considerations on BHE length that we have made
281 here concern only the lifetime cost of the plant, without taking into account the effects of very low
282 fluid temperatures. For example, if a GSHP operates at temperatures below 0°C for a sufficiently
283 long time, ground freezing can occur, and the borehole grouting can be fractured by freezing-
284 thawing cycles. In addition, the viscosity of the heat carrier fluid increases as the temperature
285 decreases, therefore the energy consumption of the circulation pump also increases. A low
286 temperature threshold should therefore be established, which excludes some of the BHE lengths
287 considered in this analysis: for example, setting a minimum inlet temperature of -3°C excludes
288 lengths below 70 m.

289
290 Although the borehole depth exerts the greatest influence on the economic balance of a BHE
291 installation, there are also other factors which have to be taken into account. In the U-pipe BHEs
292 (both single and double), which are the most diffused kind of installation, the pipes should be put as
293 far as possible, to reduce both the thermal resistance of the exchanger and the heat exchange
294 between the inlet and the outlet pipes (thermal short-circuit), which impair the performances of
295 these systems. The thermal conductivity of the borehole filling plays an important role: a higher
296 value reduces the borehole resistivity, but also the grout-to-grout resistance, which prevents the
297 thermal short-circuit. Both these factors have been taken into account in the simulations, according
298 to the borehole resistance model of Bauer et al. [34]. The distance between the pipe centres has
299 been varied between 35 mm (i.e. 3 mm between the pipe walls) and 117 mm (i.e. 0.5 mm between
300 the pipe wall and the borehole wall), and the thermal conductivity of the grout has been varied

301 between $1 \text{ Wm}^{-1}\text{K}^{-1}$ (i.e. a poor grout) and $5 \text{ Wm}^{-1}\text{K}^{-1}$ (i.e. special grouts with highly conductive
302 graphite flakes [29]). Usually, the grouts employed for BHEs have a thermal conductivity of $2\div 2.5$
303 $\text{Wm}^{-1}\text{K}^{-1}$, but this value can dramatically decrease due to an incorrect mixing, an excessive water
304 content or an insufficient concentration of thermal additives [41]. Observing the cumulate
305 distributions of the fluid temperatures (Fig.4B-C), we understand that the influence of the thermal
306 conductivity of the grout is very large when the pipe spacing is reduced; on the other hand, a grout
307 with a high thermal conductivity can compensate the negative effects of an insufficient pipe spacing
308 on both the minimum fluid temperatures and the energy consumption of the system (Fig.6B). For
309 example, if a common geothermal grout is used ($\lambda_g = 2 \text{ Wm}^{-1}\text{K}^{-1}$), the consumption of the heat
310 pump diminishes of the 1.99% as the pipe distance is increased from 35mm to 117 mm; on the other
311 hand, if a highly conductive grout ($\lambda_g = 5 \text{ Wm}^{-1}\text{K}^{-1}$) is used, this difference is reduced to the 0.64%,
312 meaning that special grouts noticeably reduce the effect of an insufficient pipe spacing.

313

314 The fluid circulated into the closed pipe loop is usually a mixture of water and antifreeze. The flow
315 rate and the physical properties of this fluid (viscosity, thermal capacity, thermal conductivity)
316 influence the borehole thermal resistance [42]. The main drawbacks of increasing the concentration
317 of the antifreeze additive are a noticeable increase of viscosity, a slight decrease of the thermal
318 conductivity and an additional cost (say $2\div 4 \text{ €/l}$, depending on the kind of ethanol or glycol); in
319 addition, the antifreeze is a potential source of contamination in case of a pipe leak, and the anti-
320 corrosion additives can inhibit the bacterial degradation [43]. All these adverse side effects should
321 be minimized when choosing the anti-freeze additive. Simulations have been carried out
322 considering the most common anti-freeze mixtures: propylene glycol (PG) at 25% and 33% volume
323 concentration, ethanol (ETH) at 24% vol., calcium chloride (CaCl_2) at 20% weight concentration.
324 Their physical properties are reported in Tab. 1, where also the boundaries of the laminar and of the
325 turbulent regime are shown, since the thermal resistance is much smaller in turbulent one [42]. The

326 default flow rate is 0.5 ls^{-1} , which is a typical value for GSHPs. The results (Fig.4D and Fig.6C)
 327 show that calcium chloride solutions permit to achieve an appraisable gain in the energy
 328 performance (compared to PG25%, minimum temperature: $+2.94^\circ\text{C}$; heat pump consumption: -
 329 4.01%), due to their smaller viscosity and their higher thermal conductivity; in addition, it is much
 330 cheaper than the other antifreeze additives. On the other hand, the use of saline solutions as a heat
 331 carrier fluid requires the adoption of specific anti-corrosion components.
 332 The other antifreeze mixtures show negligible variations of the fluid temperatures and of energetic
 333 performances. As the thermal resistance diminishes when higher flow rates are circulated, seven
 334 simulations (fluid: PG25%, flow rates: $0.1 \div 0.7 \text{ ls}^{-1}$) have been run to quantify its contribution for a
 335 better efficiency of the GSHP. We observe that the energy consumption of the heat pump is reduced
 336 of the 4.4% between 0.1 and 0.7 ls^{-1} ; nevertheless, circulating larger flow rates implies also a higher
 337 energy expense for the circulation pump. We have therefore quantified the distributed friction losses
 338 along the 75m long using the explicit approximation of the Prandtl formula (Eq.6) for smooth pipes:

339

$$\lambda_0 = \frac{0.25}{\left[\log_{10} \left(\frac{5.7}{\text{Re}^{0.9}} \right) \right]^2}$$

340 6

341 where $\lambda_0 = 2g \frac{d_{ip}}{u^2} \cdot J$ is the non dimensional friction loss, d_{ip} is the pipe internal diameter, g is the
 342 gravity acceleration, J is the hydraulic gradient in the pipes.

343 The energy consumption of the circulation pump increases rapidly with the fluid flow rate (Q_f):

344

$$CPC = \frac{J \cdot 2L \cdot \rho_f \cdot g \cdot Q_f}{\eta} \cdot t_{func} = \frac{16 \cdot \lambda_0 \cdot L \cdot \rho_f \cdot g}{\eta \cdot \pi^2 \cdot D^4} Q_f^3 \cdot t_{func}$$

345 7

346 where ρ_f is the density of the heat carrier fluid, L is the BHE length [L] and t_{func} is the operation
 347 time per year. An energy yield $\eta = 0.8$ has been assumed for the calculation of CPC .

348 Fig.8 shows the strong impact of the flow rate on the total energy consumption (circulation and heat
349 pump). In particular, a strong variation occurs when switching from laminar to transition regime
350 (between 0.2 and 0.3 l/s), with a reduction of 2.07% for the total energy consumption, while the
351 minimum values lie in a range of flow rates (for this case, 0.3÷0.5 ls⁻¹). Noticeable differences are
352 observed in the minimum temperature, meaning that higher flow rates can be adopted when larger
353 amounts of heat are extracted from the soil, in order to avoid the freezing of the ground, or to
354 reduce its extent.

355

356 While the design parameters can be determined with an acceptable precision, the real issue of
357 GSHP modelling is the knowledge of the physical parameters of the soil. The heat transport around
358 the BHE is mainly conductive, especially if no significant groundwater flow occurs, therefore the
359 most important soil physical parameter is the thermal conductivity of the porous medium λ_{ij}^{cond} (see
360 Eq.2).

361 The thermal conductivity of the solid matrix (λ_s) is the parameter which can vary in the widest
362 range, depending on the lithology, the grain size, the water saturation etc.. A wide range of values
363 has been explored in the simulations (1÷3 Wm⁻¹K⁻¹), and the graphs of the cumulate distribution of
364 the fluid temperatures (Fig.5E) and of the heat pump energy consumption (Fig.6D) show that
365 thermal conductivity has a very strong influence on the performances of the system, compared to
366 the BHE length. Especially in smaller installations, this parameter is not measured in situ, but low-
367 precision data from literature are adopted (e.g. the German norm VDI 4640 [44]). For example, the
368 thermal conductivity of a moraine ranges between 1 and 2.5 Wm⁻¹K⁻¹, for which we observe a
369 difference of 5.66°C in the minimum temperature, and 12.5% in the power consumed by the heat
370 pump. An imprecise knowledge of this parameter results therefore in a strong uncertainty in the
371 simulation of the plant, which has to be overcome e.g. with a Thermal Response Test [45].

372

373 The presence of a subsurface flow has been proved to be beneficial for the performances of closed-
374 loop geothermal heat pumps. Indeed, groundwater flow activates advection and thermal dispersion,
375 enhancing the heat transport around the BHE and spreading the thermal disturbance further away.
376 Chiasson et al. [25] demonstrated that the advection has a considerable impact only in coarse-
377 grained soil (sands and gravels) and in fractured aquifers (e.g. karst limestone), while Wang et al.
378 [26] stressed the importance of the saturated thickness, which can vary through the year, influencing
379 also the results of Thermal Response Tests [12]. A set of simulations with different flow velocities
380 and saturated thicknesses has been run therefore to quantify the positive effect of groundwater flow
381 in a typical sand aquifer ($K = 10^{-4} m/s$).

382 As shown in Fig.5B-C and Fig.6E, the influence of the Darcy velocity on the performances of the
383 system is much stronger than the variation induced by different saturated thicknesses. This means
384 that the contribution of the advection can be taken into account, but precise values are needed to
385 avoid undersized design; on the other hand, variations in the saturated thickness - e.g. due to
386 seasonal level variations in surface water bodies - do not exert a strong influence on the operation
387 of GSHPs, if the gradient does not experience significant variations.

388
389 When modelling heat transport in an aquifer, one should consider also the dispersion, which is a
390 strong mechanism of heat transport. The thermal dispersivity has been considered as a scale-
391 dependent parameter, as reported in literature [46]. Sethi and Di Molfetta [21] adopted $\alpha_L = 10 m$
392 and $\alpha_T = 1 m$ for the heat transport simulation around a municipal solid waste landfill. Erol [47]
393 assumed $\alpha_L = 2 m$ and $\alpha_T = 0.2 m$ for the simulation of a 100 m long BHE. Molina-Giraldo et al.
394 [48] analyzed the extension of the thermal plume downstream of a BHE, for different values of
395 groundwater flow Darcy velocity ($q = 10^{-8} \div 10^{-5} m/s$) and for different values of thermal
396 dispersivity ($\alpha_L = 0 \div 2 m$), discovering that thermal dispersion reduces the extent of a reference
397 isotherm (e.g. $+1^\circ C$) of the deviation from the undisturbed soil temperature.

398 Wagner et al. [49] also analyzed the effect of α_L for Thermal Response Tests in presence of
399 groundwater flow, concluding that thermal dispersion can lead to a strong overestimation of the
400 thermal conductivity of the soil. This is confirmed by the cumulate distribution of the average fluid
401 temperatures for a Darcy velocity of 4.32 m/day (Fig.5D), which prove that the thermal dispersion
402 is a great factor of uncertainty when modelling BHE fields in presence of subsurface flow. A rule of
403 thumb that is usually employed in the solute transport [50] is:

$$404 \quad \alpha_L = 0.1L_p$$

405 8

406 where L_p is the spatial scale of the dispersion phenomenon. The concept of “scale” is not
407 univocally defined for GSHPs: using the BHE diameter (i.e. $\alpha_L = 0.1m$ or less) or its length (i.e.
408 $\alpha_L = 10m$) would imply a difference of some $8\div 10^\circ\text{C}$ for the minimum fluid temperature and more
409 than 15% for the electricity consumption of the heat pump (see Fig.6F). It is therefore advised not
410 to rely on thermal dispersion when designing BHE fields, until field tests will be carried to estimate
411 the thermal dispersivity in real-scale setups: especially if a thick and conductive aquifer is present,
412 the overestimation of the thermal dispersivity would lead to an under-dimensioning of the GSHP
413 with a detrimental effect on its long-term sustainability.

414

415 **4. Conclusions**

416 In this work, the most important parameters which influence the performances of Ground Source
417 Heat Pumps have been thoroughly analyzed, running long-term simulations and estimating the
418 energy consumption of the heat pump for each setting. Most of these factors have been already
419 analyzed in other works, but none of them considered all the parameters together, using the same
420 modelling framework and considering the effect on the lifetime of a GSHP. The analysis of the
421 BHE design parameters (length, pipe spacing, fluid, grout) permits to understand which are the
422 margins of improvement, while the physical parameters of the soil (thermal conductivity and

423 dispersivity, groundwater flow) have been analyzed in order to understand their effect on the
424 uncertainty in the project phase.

425 The results of the simulations prove that the length of the BHE is the most important parameter in
426 the design of a GSHP. Indeed, increasing the borehole depth results in a reduction of the thermal
427 disturbance in the subsoil and therefore to achieve a higher efficiency of the heat pump, but also a
428 larger investment is needed for the installation.

429 An optimum length should be found, which minimizes the total cost over the plant lifetime,
430 considering also the trend of increase of the unit cost of electricity. While the drilled depth has an
431 appraisable impact on the initial investment, there are also other important factors to be considered
432 for the optimization of BHEs, like the pipe arrangement, the grout and the heat carrier fluid. A large
433 pipe spacing and a highly conductive grout, reducing the heat losses in the heat exchange with the
434 soil, achieves an appraisable reduction of the energy costs for the heat pump with a negligible
435 expense, compared to the borehole drilling. For the circulation pump, a trade-off can be found for
436 the choice of the correct flow rate for the heat carrier fluid, allowing the minimization of both the
437 energy losses due to the thermal resistance and the friction losses due to the circulation of the fluid.
438 The antifreeze and its concentration heavily influence the energy performance of GSHPs, in
439 particular the borehole resistance and the power consumed by the auxiliary plants. The saline
440 solutions, with a smaller viscosity compared to ethanol and glycols, permit to reduce all these
441 energy losses, although special components are needed to avoid corrosion problems. Optimizing the
442 design and the installation of BHEs is useless without a thorough characterization of the subsoil,
443 which has a large influence on the performances of these systems. When no groundwater flow
444 occurs, the thermal conductivity is the most important parameter for the dimensioning of BHEs.
445 The technical literature provides wide ranges of the thermal conductivity for each lithology, which
446 can vary due to porosity, saturation and other factors; in-situ Thermal Response Tests are therefore
447 strongly advised for large plants to avoid under or over dimensioning. The advection enhances the
448 performances of GSHP, and the groundwater flow should be taken into account using conservative

449 values of hydraulic conductivity and gradient, unless they are known by field tests. On the other
450 hand, it is risky to consider also the beneficial effect of heat dispersion, because the thermal
451 dispersivity is still scarcely known in real-scale BHEs. In situ tests to estimate these parameters
452 would be highly desirable to simulate the behaviour of BHE fields with a better precision.

453 **References**

- 454 [1] R. Curtis, J. Lund, B. Sanner, L. Rybach, G. Hellstrom, Ground Source Heat Pumps -
455 Geothermal Energy for Anyone, Anywhere: Current Worldwide Activity, in: World Geothermal
456 Congress, Antalya (Turkey), 2005, pp. 9.
- 457 [2] EUROBSERV'ER, The state of renewable energies in Europe - 11th EurObserv'ER Report, in,
458 EUROBSERV'ER, 2011, pp. 254.
- 459 [3] W. Goetzler, R. Zogg, H. Lisle, J. Burgos, Ground-source heat pumps: overview of the market
460 status, barriers to adoption, and options for overcoming barriers, in, U.S. Department of Energy,
461 2009.
- 462 [4] D. Saner, R. Juraske, M. Kübert, P. Blum, S. Hellweg, P. Bayer, Is it only CO₂ that matters? A
463 life cycle perspective on shallow geothermal systems, *Renewable and Sustainable Energy Reviews*,
464 14 (2010) 1798-1813.
- 465 [5] P.F. Healy, V.I. Ugursal, Performance and economic feasibility of ground source heat pumps in
466 cold climate, *International Journal of Energy Research*, 21 (1997) 857-870.
- 467 [6] V. Badescu, Economic aspects of using ground thermal energy for passive house heating,
468 *Renewable Energy*, 32 (2007) 895-903.
- 469 [7] S. Blumsack, A. Kleit, S.W. Smith, Evaluation of federal and state subsidies for ground-source
470 heat pumps, *Energy Efficiency*, 5 (2012) 321-334.
- 471 [8] L.R. Ingersoll, Theory of the ground pipe source for the heat pump, *ASHVE Transactions*, 54
472 (1948) 339-348.
- 473 [9] H.G. Carslaw, J.C. Jaeger, *Conduction of heat in solids*, Cambridge, UK, 1946.
- 474 [10] D. Marcotte, P. Pasquier, F. Sheriff, M. Bernier, The importance of axial effects for borehole
475 design of geothermal heat-pump systems, *Renewable Energy*, 35 (2010) 763-770.
- 476 [11] H.J.L. Witte, Error analysis of thermal response tests, *Applied Energy*, 109 (2013) 302-311.
- 477 [12] Ş. Bozdağ, B. Turgut, H. Paksoy, D. Dikici, M. Mazman, H. Evliya, Ground water level
478 influence on thermal response test in Adana, Turkey, *International Journal of Energy Research*, 32
479 (2008) 629-633.
- 480 [13] V. Wagner, P. Blum, M. Kübert, P. Bayer, Analytical approach to groundwater-influenced
481 thermal response tests of grouted borehole heat exchangers, *Geothermics*, 46 (2013) 22-31.
- 482 [14] P. Eskilson, *Thermal Analysis of Heat Extraction Boreholes*, in, Lund University (Sweden),
483 1987.
- 484 [15] G. Hellstrom, B. Sanner, *Earth Energy Designer, User Manual Version 2.0*, 2000.
- 485 [16] J.D. Spitler, GLHEPRO - A design tool for commercial building ground loop heat exchangers,
486 in: 4th International Heat Pumps in Cold Climates Conference, Aylmer, Quebec, 2000.
- 487 [17] N. Diao, Q. Li, Z. Fang, Heat transfer in ground heat exchangers with groundwater advection,
488 *International Journal of Thermal Sciences*, 43 (2004) 1203-1211.
- 489 [18] T.V. Bandos, Á. Montero, E. Fernández, J.L.G. Santander, J.M. Isidro, J. Pérez, P.J.F.d.
490 Córdoba, J.F. Urchueguía, Finite line-source model for borehole heat exchangers: effect of vertical
491 temperature variations, *Geothermics*, 38 (2009) 263-270.
- 492 [19] N. Molina-Giraldo, P. Blum, K. Zhu, P. Bayer, Z. Fang, A moving finite line source model to
493 simulate borehole heat exchangers with groundwater advection, *International Journal of Thermal
494 Sciences*, 50 (2011) 2506-2513.
- 495 [20] J. Hecht-Mendez, N. Molina-Giraldo, P. Blum, P. Bayer, Evaluating MT3DMS for Heat
496 Transport Simulation of Closed Geothermal Systems, *Ground Water*, 48 (2010) 741-756.
- 497 [21] R. Sethi, A. Di Molfetta, Heat transport modeling in an aquifer downgradient a municipal solid
498 waste landfill in Italy, *American Journal of Environmental Sciences*, 3 (2007) 106-110.
- 499 [22] C.D. Langevin, D.T. Thorne, A.M. Dausman, M.C. Sukop, W. Guo, SEAWAT Version 4: A
500 Computer Program for Simulation of Multi-Species Solute and Heat Transport, in: USGS (Ed.) U.S.
501 Geological Survey Techniques and Methods, 2008, pp. 39.

502 [23] H.J.G. Diersch, D. Bauer, W. Heidemann, W. Rühaak, P. Schätzl, Finite element modeling of
503 borehole heat exchanger systems: Part 1. Fundamentals, *Computers and Geosciences*, 37 (2011)
504 1122-1135.

505 [24] H.J.G. Diersch, D. Bauer, W. Heidemann, W. Rühaak, P. Schätzl, Finite element modeling of
506 borehole heat exchanger systems. Part 2. Numerical simulation, *Computers and Geosciences*, 37
507 (2011) 1136-1147.

508 [25] A.C. Chiasson, S.J. Rees, J.D. Spitler, A Preliminary Assessment of the Effects of Ground-
509 Water Flow on Closed-Loop Ground-Source Heat Pump Systems, *ASHRAE Transactions*, 106
510 (2000) 380-393.

511 [26] H.J. Wang, C.Y. Qi, H.P. Du, J.H. Gu, Thermal performance of borehole heat exchanger under
512 groundwater flow: A case study from Baoding, *Energy and Buildings*, 41 (2009) 1368-1373.

513 [27] C.K. Lee, Effects of multiple ground layers on thermal response test analysis and ground-
514 source heat pump simulation, *Applied Energy*, 88 (2011) 4405-4410.

515 [28] J.T. Chung, J.M. Choi, Design and performance study of the ground-coupled heat pump
516 system with an operating parameter, *Renewable Energy*, 42 (2012) 118-124.

517 [29] F. Delaleux, X. Py, R. Olives, A. Dominguez, Enhancement of geothermal borehole heat
518 exchangers performances by improvement of bentonite grouts conductivity, *Applied Thermal
519 Engineering*, 33-34 (2012) 92-99.

520 [30] L. Jun, Z. Xu, G. Jun, Y. Jie, Evaluation of heat exchange rate of GHE in geothermal heat
521 pump systems, *Renewable Energy*, 34 (2009) 2898-2904.

522 [31] A. Michopoulos, N. Kyriakis, The influence of a vertical ground heat exchanger length on the
523 electricity consumption of the heat pumps, *Renewable Energy*, 35 (2010) 1403-1407.

524 [32] H.J.G. Diersch, O. Kolditz, *FEFLOW Reference Manual*, DHI-Wasy, Berlin, 2002.

525 [33] H.J.G. Diersch, O. Kolditz, *FEFLOW 6 User Manual*, DHI-Wasy, Berlin, 2010.

526 [34] D. Bauer, W. Heidemann, H. Müller-Steinhagen, H.J.G. Diersch, Thermal resistance and
527 capacity models for borehole heat exchangers, *International Journal of Energy Research*, 35 (2011)
528 312-320.

529 [35] P. Eskilson, J. Claesson, Simulation model for thermally interacting heat extraction boreholes,
530 *Numerical Heat Transfer*, 13 (1988) 149-165.

531 [36] R. Al-Khoury, P.G. Bonnier, Efficient finite element formulation for geothermal heating
532 systems. Part II: Transient, *International Journal for Numerical Methods in Engineering*, 67 (2006)
533 725-745.

534 [37] R. Al-Khoury, P.G. Bonnier, R.B.J. Brinkgreve, Efficient finite element formulation for
535 geothermal heating systems. Part I: Steady state, *International Journal for Numerical Methods in
536 Engineering*, 63 (2005) 988-1013.

537 [38] H.-J.G. Diersch, D. Bauer, W. Heidemann, W. Ruhaak, P. Schatzl, Finite element formulation
538 for borehole heat exchangers in modeling geothermal heating systems by FEFLOW, in: *DHI-
539 WASY (Ed.) FEFLOW White Papers*, Berlin, 2010.

540 [39] H.N. Pollack, S.J. Hurter, J.R. Johnson, Heat flow from the earth's interior: analysis of the
541 global data set, *Reviews of Geophysics*, 31 (1993) 267-280.

542 [40] P. Blum, G. Campillo, T. Kölbl, Techno-economic and spatial analysis of vertical ground
543 source heat pump systems in Germany, *Energy*, 36 (2011) 3002-3011.

544 [41] C. Lee, K. Lee, H. Choi, H.P. Choi, Characteristics of thermally-enhanced bentonite grouts for
545 geothermal heat exchanger in South Korea, *Sci China Technol Sc*, 53 (2010) 123-128.

546 [42] D. Bauer, W. Heidemann, H. Müller-Steinhagen, H.J.G. Diersch, Thermal resistance and
547 capacity models for borehole heat exchangers, *International Journal of Energy Research*, (2010)
548 n/a-n/a.

549 [43] T. Klotzbücher, A. Kappler, K.L. Straub, S.B. Haderlein, Biodegradability and groundwater
550 pollutant potential of organic anti-freeze liquids used in borehole heat exchangers, *Geothermics*, 36
551 (2007) 348-361.

552 [44] VDI, VDI 4640 - Thermal use of underground, in: Blatt 1: Fundamentals, approvals,
553 environmental aspects, 2000.

554 [45] S. Gehlin, Thermal Response Test - Method Development and Evaluation, in: Department of
555 Environmental Engineering, Lulea University of Technology, Lulea (Sweden), 2002, pp. 191.

556 [46] G. de Marsily, Quantitative hydrogeology, Academic Press, San Diego (CA, USA), 1986.

557 [47] S. Erol, Estimation of heat extraction rates of GSHP systems under different hydrogeological
558 conditions, in, University of Tübingen, 2011.

559 [48] N. Molina-Giraldo, P. Bayer, P. Blum, Evaluating the influence of thermal dispersion on
560 temperature plumes from geothermal systems using analytical solutions, International Journal of
561 Thermal Sciences, 50 (2011) 1223-1231.

562 [49] V. Wagner, P. Bayer, M. Kübert, P. Blum, Numerical sensitivity study of thermal response
563 tests, Renewable Energy, 41 (2012) 245-253.

564 [50] A. Di Molfetta, R. Sethi, Ingegneria degli Acquiferi, Springer, 2012.

565

566

567 **Nomenclature**

568	BHL	Total annual BHE Heat Load (kWh y^{-1})
569	BHL_i	BHE Heat Load at the i -th time step (kW)
570	c_f	Groundwater specific heat ($\text{J kg}^{-1} \text{K}^{-1}$)
571	c_s	Aquifer solid matrix specific heat ($\text{J kg}^{-1} \text{K}^{-1}$)
572	COP	Coefficient of Performance of the heat pump (dimensionless)
573	CPC	Circulating Pump Consumption (kWh y^{-1})
574	d_{ip}	Internal pipe diameter (m)
575	d_{op}	External pipe diameter (m)
576	g	Gravity acceleration (m s^{-2})
577	H	Heat source/sink (W/m^3)
578	HPC	Total annual Heat pump energy consumption (kW y^{-1})
579	HPC_i	Power consumed by the heat pump at the i -th time step (kW)
580	$-\frac{\partial h}{\partial x}$	Hydraulic gradient in the aquifer (dimensionless)
581	J	Hydraulic gradient in the BHE pipes (dimensionless)
582	K	Hydraulic conductivity of the aquifer (m s^{-1})
583	L	Length of the BHE (m)
584	L_p	Scale dimension (m)
585	n_e	Effective porosity or specific yield of the aquifer (dimensionless)
586	Q_f	Flow rate of the heat carrier fluid (l s^{-1})
587	q	Darcy velocity of groundwater flow (m s^{-1})
588	q_i	i -th component of the Darcy velocity (m s^{-1})

589	Re	Reynolds number (dimensionless)
590	RMSE	Root Mean Square Error
591	T	Temperature of the soil, both solid and fluid phase ($^{\circ}\text{C}$)
592	T_f	Average fluid temperature ($^{\circ}\text{C}$)
593	t_{func}	Functioning time of the circulation pump (d y^{-1})
594	T_{in}	Inlet fluid temperature ($^{\circ}\text{C}$)
595	T_{out}	Outlet fluid temperature ($^{\circ}\text{C}$)
596	T_s	Soil temperature at the borehole interface ($^{\circ}\text{C}$)
597	u	Flow velocity in the BHE pipes (m s^{-1})
598	w	Distance between the centres of the pipes in a BHE (m)
599	Greek letters	
600	α_L	Longitudinal thermal dispersivity (m)
601	α_T	Transverse thermal dispersivity (m)
602	ε	Porosity of the soil (dimensionless)
603	η	Energy yield (dimensionless)
604	λ_0	Non-dimensional friction loss (dimensionless)
605	λ_f	Thermal conductivity of the heat carrier fluid ($\text{W m}^{-1} \text{K}^{-1}$)
606	λ_g	Thermal conductivity of the grout ($\text{W m}^{-1} \text{K}^{-1}$)
607	λ_p	Thermal conductivity of the BHE pipes ($\text{W m}^{-1} \text{K}^{-1}$)
608	λ_s	Thermal conductivity of the solid matrix of the soil ($\text{W m}^{-1} \text{K}^{-1}$)
609	λ_w	Groundwater thermal conductivity ($\text{W m}^{-1} \text{K}^{-1}$)
610	λ_{ij}^{cond}	Thermal conductivity for conduction ($\text{W m}^{-1} \text{K}^{-1}$)

611	λ_{ij}^{disp}	Thermal conductivity for dispersion ($\text{W m}^{-1} \text{K}^{-1}$)
612	ρ_f	Density of the heat carrier fluid (Kg m^{-3})
613	ρ_s	Density of the solid matrix of the soil (Kg m^{-3})
614	ρ_w	Density of groundwater (Kg m^{-3})
615	$(\rho c)_f$	Thermal capacity of the heat carrier fluid ($\text{J m}^{-3} \text{K}^{-1}$)
616	$(\rho c)_g$	Thermal capacity of the grout ($\text{J m}^{-3} \text{K}^{-1}$)
617	$(\rho c)_s$	Thermal capacity of the solid matrix of the soil ($\text{J m}^{-3} \text{K}^{-1}$)
618	$(\rho c)_w$	Thermal capacity of the solid matrix of the soil ($\text{J m}^{-3} \text{K}^{-1}$)

619 **Tables**

Fluid	$T_{freezing}$ [°C]	λ_f [Wm ⁻¹ K ⁻¹]	c_f [Jkg ⁻¹ K ⁻¹]	ρ_f [kgm ⁻³]	μ_f [mPas]	Q_{lam} [Is ⁻¹]	Q_{turb} [Is ⁻¹]
Prop.Glycol 25%	-10	0.45	3974	1026	5.51	0.252	1.097
Ethanol 24.4%	-15	0.426	4288	972	5.85	0.283	1.229
Prop.Glycol 33%	-15	0.416	3899	1015	8.17	0.378	1.644
CaCl ₂ 20%	-20	0.54	3030	1186	4	0.158	0.689

620

621 **Tab. 1 – Physical properties of the anti-freeze solutions used in the simulations: solidification temperature**
 622 **($T_{freezing}$), thermal conductivity (λ_f), specific heat (c_f), density (ρ_f), dynamic viscosity (μ_f), upper boundary**
 623 **flow rate for the laminar regime (Q_{lam}) and lower boundary flow rate for the turbulent regime (Q_{turb}).**

624

Parameter	Values
6 kW heat pump + installation	6000€
BHE drilling + installation	70 €/m
Unit cost of electricity	0.22 €/kWh
Increment of the unit cost of electricity	0%, 1%, 3%, 5%

625

626 **Tab. 2 – Installation and energy costs used for the optimization procedure of the BHE length.**

627

628 **Figure captions**

629 **Fig. 1 – Scheme of a Ground Source Heat Pump (GSHP): the Borehole Heat Exchanger (BHE) exchanges heat**
 630 **between the surrounding soil and the heat pump. A thermal storage tank reduces the frequency of start-up and**
 631 **stop of the heat pump. Radiant panels and fan coils are the most diffused heating terminals for GSHPs. If**
 632 **present, groundwater flow enhances the heat transport around the BHE, permitting to achieve better energy**
 633 **performances.**

634

635 **Fig. 2 – Building Heat Load (BHL) adopted as a benchmark for the BHE in the simulations.**

636

637 **Fig. 3 – A: Time series of the average fluid temperatures, detail of 5 years of simulation. B: Cumulate**
638 **distribution of the average fluid temperatures in the heating seasons.**

639

640 **Fig. 4 – Cumulate distributions of the average fluid temperatures for different values of BHE length (A), pipe**
641 **spacing (B), thermal conductivity of the grout (C) and heat carrier fluids (D).**

642

643 **Fig. 5 – Cumulate distributions of the average fluid temperatures for different values of the thermal conductivity**
644 **of the solid matrix of the soil (A), groundwater flow Darcy velocity with no thermal dispersion (B), Darcy**
645 **velocity and saturated thickness (C), thermal dispersivity (D).**

646

647 **Fig. 6 – Estimated annual heat pump energy consumption for different values of BHE length (A), pipe spacing**
648 **and grout conductivity (B), heat carrier fluids (C), solid-phase soil thermal conductivity (D), groundwater flow**
649 **Darcy velocity and saturated thickness (E) and thermal dispersivity (F).**

650

651 **Fig. 7 – Relative variation of the total cost of a GSHP over a lifetime of 30 years, for different BHE lengths**
652 **(50÷100m) and different increment rates of the unit cost of electricity (0÷5%).**

653

654 **Fig. 8 – Cumulate distributions of the average fluid temperatures (A) and electric power consumption of the heat**
655 **pump and circulation pump (B) for different fluid flow rates.**

Supporting information

Tab. 1 – Summary of the results of the simulations: mean and RMSE of the average fluid temperature (T_f), minimum values of the inlet temperature (T_{in}), Seasonal Performance Factor (SPF) and annual Heat Pump Consumption (HPC).

Parameter	value	Parameter	value	mean (T_f) [°C]	RMSE (T_f) [°C]	min (T_{in}) [°C]	SPF [-]	HPC [kWh/y]
		BHE length [m]	50	1.83	5.69	-6.39	4.22	2845.8
			55	2.52	5.36	-5.34	4.29	2799.5
			60	3.07	5.01	-4.40	4.34	2765.6
			65	3.46	4.79	-3.94	4.37	2743.0
			70	4.14	4.54	-2.99	4.44	2704.0
			75	4.63	4.25	-2.24	4.48	2678.4
			80	4.99	4.06	-1.71	4.51	2661.4
			85	5.26	3.92	-1.49	4.53	2648.5
			90	5.62	3.76	-1.02	4.56	2631.3
			95	6.03	3.57	-0.47	4.60	2611.1
			100	6.21	3.46	-0.33	4.61	2604.2
pipe spacing [mm]	35	grout thermal conductivity [$\text{Wm}^{-1}\text{K}^{-1}$]	1	0.34	7.16	-10.02	4.06	2956.2
	35		2	3.88	4.85	-3.74	4.42	2715.9
	35		3	4.18	4.59	-3.22	4.44	2701.2
	35		5	4.65	4.27	-2.27	4.48	2678.4
	55		1	0.62	6.92	-9.43	4.09	2931.5

Parameter	value	Parameter	value	mean (T_f) [°C]	RMSE (T_f) [°C]	min (T_{in}) [°C]	SPF [-]	HPC [kWh/y]
	55		2	4.05	4.74	-3.46	4.43	2706.4
	55		3	4.29	4.49	-3.04	4.45	2695.5
	55		5	4.64	4.25	-2.20	4.48	2678.0
	80		1	1.32	6.39	-7.95	4.17	2877.8
	80		2	4.20	4.55	-3.10	4.45	2699.6
	80		3	4.60	4.27	-2.31	4.48	2680.9
	80		5	4.68	4.17	-2.06	4.48	2677.7
	100		1	4.23	4.77	-3.41	4.45	2695.1
	100		2	4.74	4.33	-2.33	4.49	2670.7
	100		3	4.67	4.18	-2.09	4.48	2677.6
	100		5	4.74	4.05	-1.97	4.48	2676.9
	117		1	3.09	4.95	-4.29	4.34	2766.9
	117		2	5.03	3.90	-1.36	4.51	2661.9
	117		3	5.07	3.86	-1.31	4.51	2660.7
	117		5	5.07	3.84	-1.32	4.51	2661.3
		heat carrier fluid	PG 33%	1.95	5.96	-6.74	4.23	2834.8
			ET 24%	1.98	5.79	-6.49	4.23	2835.0
			PG 25%	2.49	5.50	-5.62	4.29	2799.7
			CaCl ₂ 20%	4.43	4.43	-2.68	4.47	2687.4
		solid matrix thermal conductivity [Wm ⁻¹ K ⁻¹]	1	-0.63	6.08	-9.36	3.91	3072.7
			1.5	1.32	5.47	-6.86	4.14	2895.8
			2	2.73	4.99	-4.72	4.30	2790.5

Parameter	value	Parameter	value	mean (T_f) [°C]	RMSE (T_f) [°C]	min (T_{in}) [°C]	SPF [-]	HPC [kWh/y]
			2.5	3.60	4.64	-3.70	4.38	2737.5
			3	4.63	4.25	-2.24	4.48	2678.4
saturated thickness [m]	55	groundwater flow Darcy velocity [m/d]	0.864	5.28	4.37	-1.83	4.54	2640.8
			1.728	5.99	4.37	-1.39	4.61	2601.0
			1.32	6.85	4.17	-0.33	4.70	2552.5
			8.64	7.53	3.77	0.80	4.76	2520.7
			17.28	8.21	3.29	2.14	4.82	2491.9
groundwater flow Darcy velocity [m/d]	0.864	saturated thickness [m]	10	4.67	4.32	-2.27	4.48	2676.2
			20	4.91	4.31	-2.06	4.51	2662.4
			50	5.25	4.36	-1.83	4.54	2642.6
groundwater flow Darcy velocity [m/d]	8.64	saturated thickness [m]	10	5.73	4.23	-1.20	4.59	2615.7
			20	6.43	4.07	-0.54	4.66	2576.8
			50	7.41	3.82	0.62	4.75	2526.6
groundwater flow Darcy velocity [m/d]	0.864	longitudinal thermal dispersivity [m]	0.1	5.32	4.35	-1.82	4.55	2639.0
			0.2	5.35	4.33	-1.81	4.55	2637.7
			0.5	5.46	4.27	-1.74	4.56	2632.0
			1	5.61	4.20	-1.35	4.57	2624.1
			2	5.72	4.11	-1.26	4.58	2619.1
			5	6.32	3.78	-0.44	4.63	2589.9
groundwater flow Darcy velocity [m/d]	1.728	longitudinal thermal dispersivity [m]	0.1	6.04	4.34	-1.32	4.62	2598.7
			0.2	6.10	4.30	-1.27	4.62	2596.1
			0.5	6.23	4.20	-0.89	4.63	2589.8

Parameter	value	Parameter	value	mean (T_f) [°C]	RMSE (T_f) [°C]	min (T_{in}) [°C]	SPF [-]	HPC [kWh/y]
			1	6.43	4.08	-0.80	4.65	2580.5
			2	6.62	3.91	-0.37	4.67	2572.3
			5	7.48	3.39	1.16	4.74	2534.0
groundwater flow Darcy velocity [m/d]	4.32	longitudinal thermal dispersivity [m]	0.1	6.91	4.14	-0.29	4.71	2550.0
			0.2	6.98	4.09	-0.26	4.71	2547.1
			0.5	7.26	3.91	0.29	4.73	2535.4
			1	7.60	3.68	0.93	4.76	2521.6
			2	8.09	3.33	1.86	4.80	2501.3
			5	8.94	2.78	3.44	4.86	2467.8

Tab. 2 – Summary of the results of the simulations with different values of heat carrier fluid flow rate (Q_f): mean and RMSE of the average fluid temperature (T_f), minimum values of the inlet temperature (T_{in}), Seasonal Performance Factor (SPF), annual heat pump consumption (HPC), circulating pump energy consumption (CPC) and total energy consumption (HPC+CPC).

Q_f [l/s]	mean (T_f) [°C]	RMSE (T_f) [°C]	min (T_{in}) [°C]	SPF	HPC [kWh/y]	CPC [kWh/y]	HPC+CPC [kWh/y]
0.1	-0.52	7.34	-16.57	4.09	2932.4	1.3	2933.8
0.2	0.19	7.02	-11.68	4.13	2906.6	8.2	2914.8
0.3	1.71	5.96	-7.51	4.24	2830.6	24.0	2854.6
0.4	2.49	5.50	-5.62	4.29	2799.7	51.9	2851.6
0.5	2.76	5.24	-4.97	4.28	2800.9	94.5	2895.4
0.6	3.14	4.99	-4.17	4.30	2790.8	154.5	2945.3
0.7	3.14	4.94	-3.75	4.28	2803.1	234.4	3037.5

Fig.1

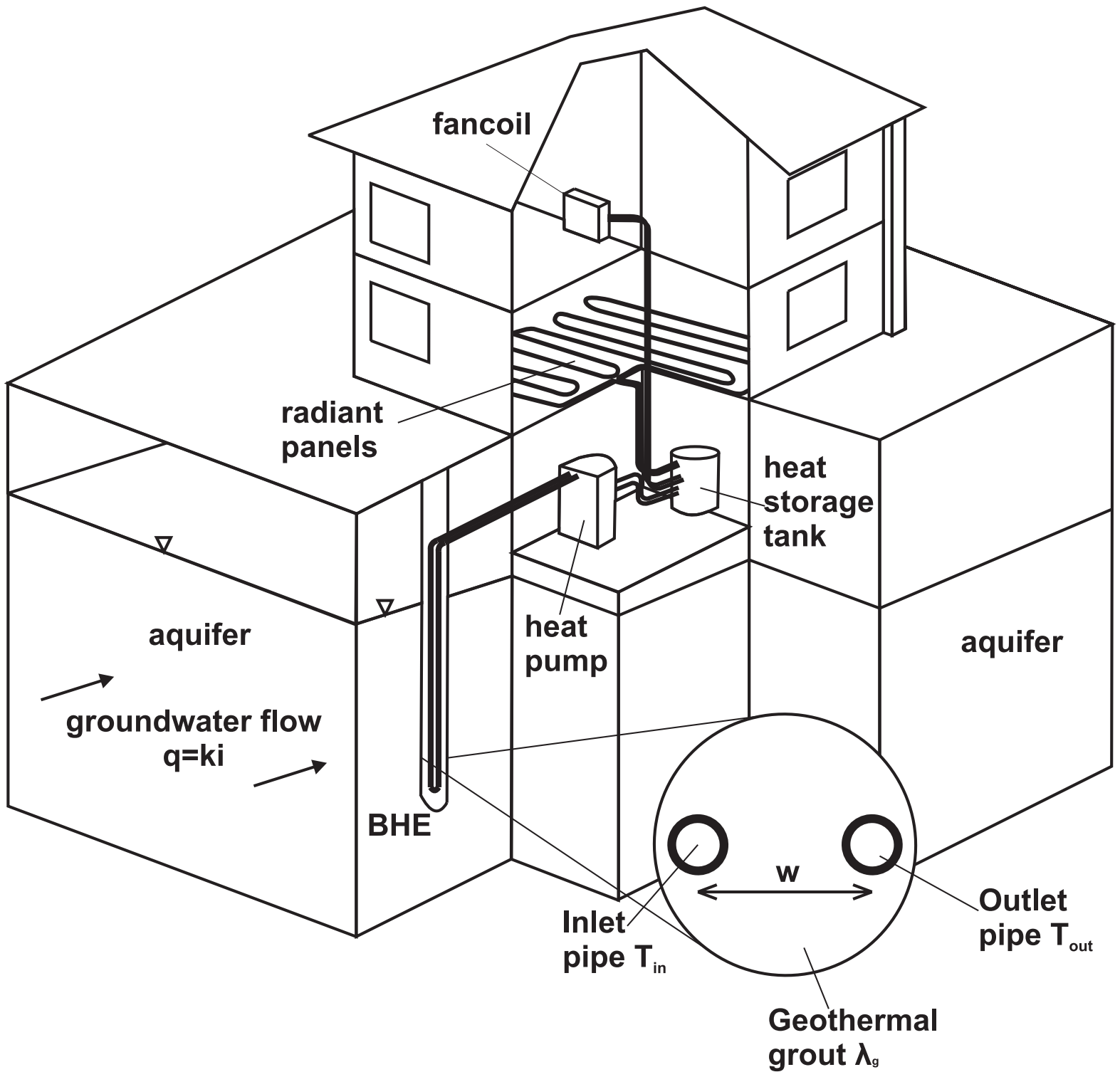


Fig.2

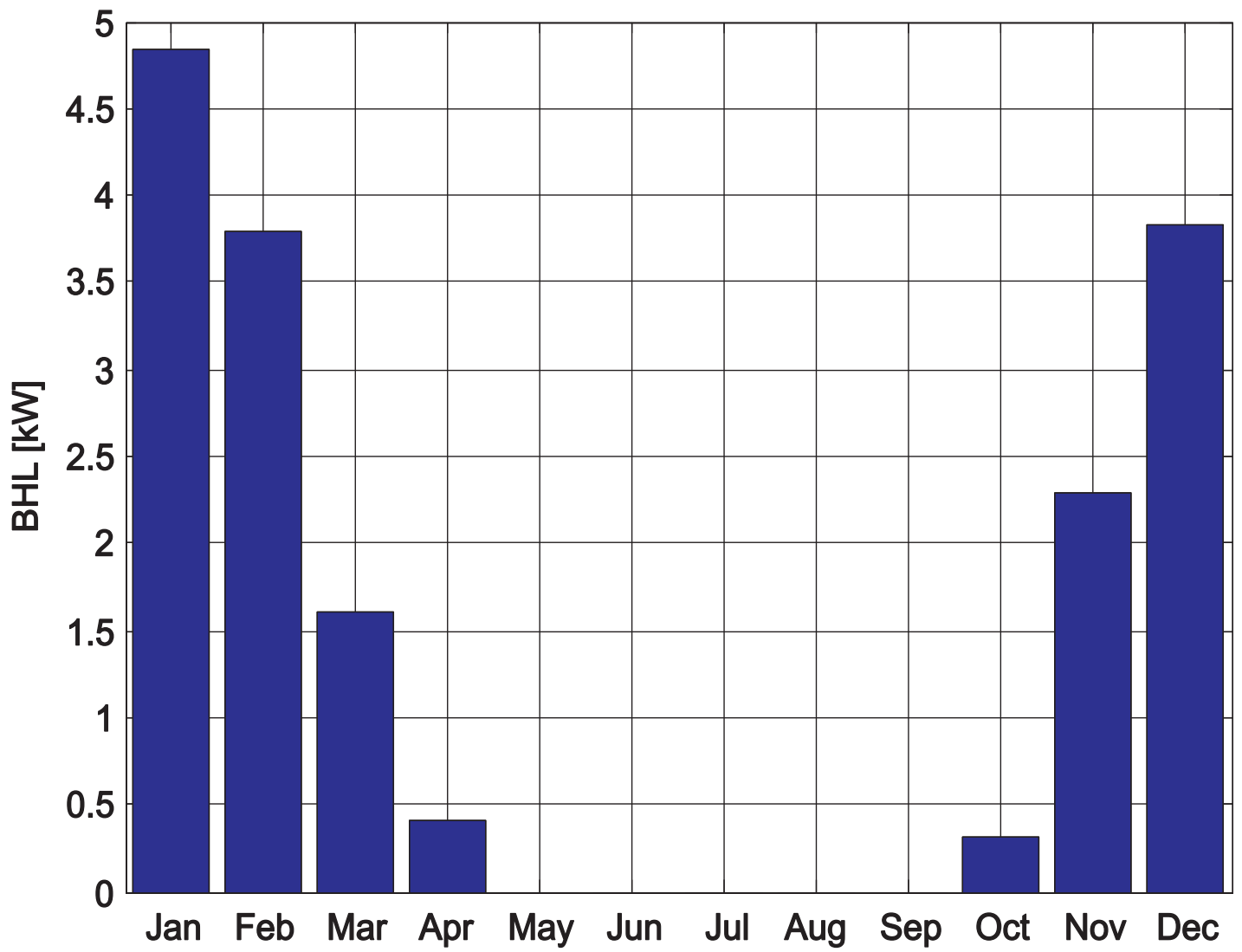


Fig.3

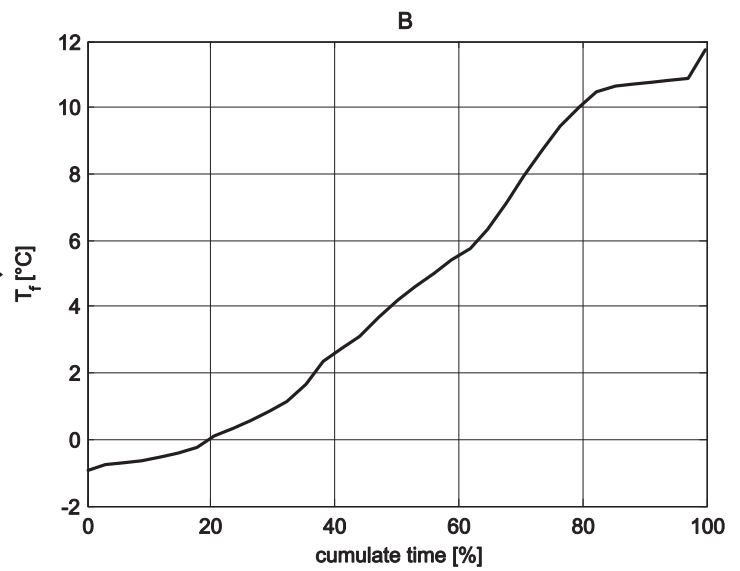
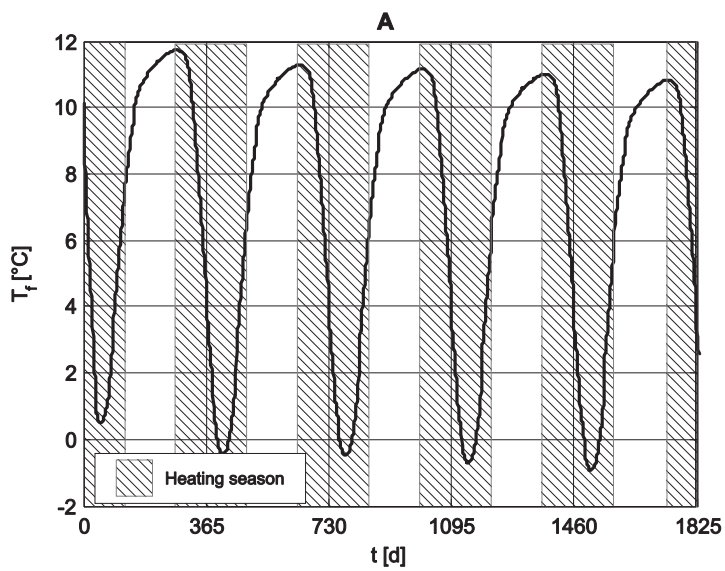


Fig.4

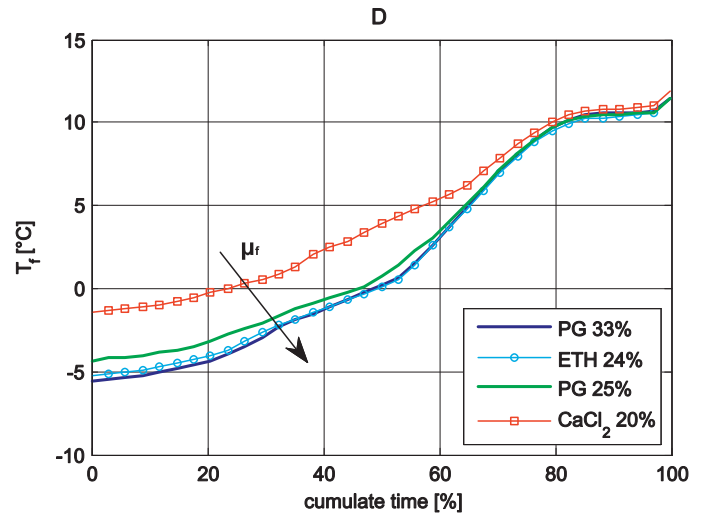
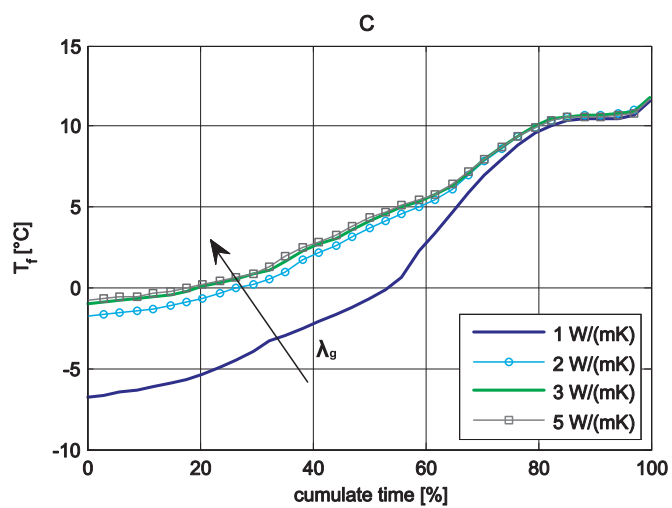
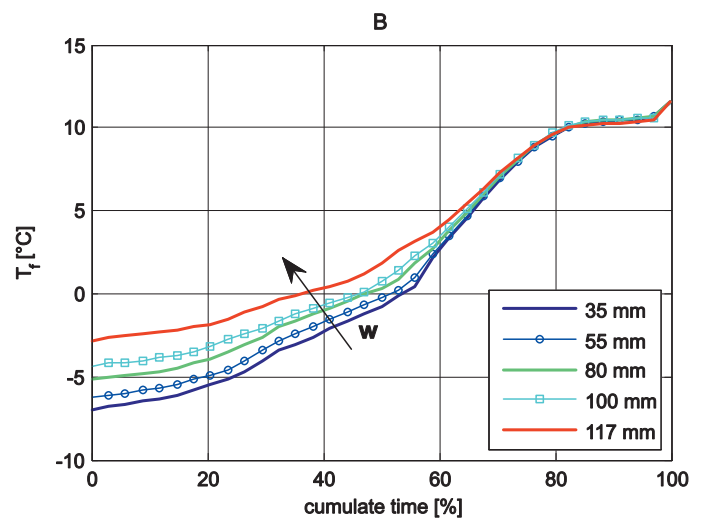
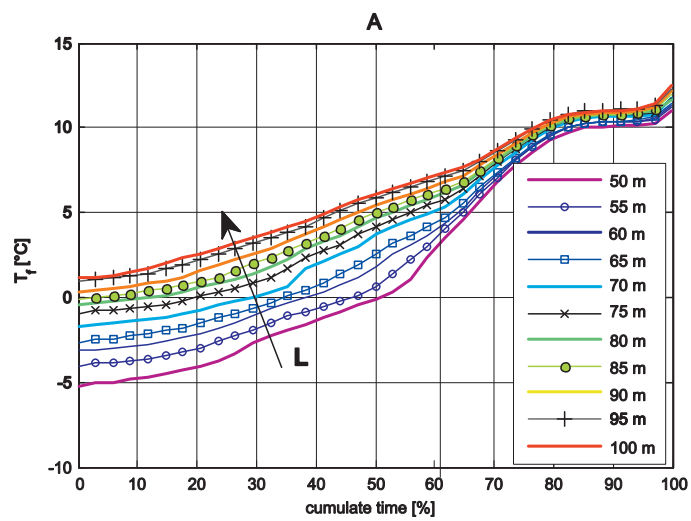


Fig.5

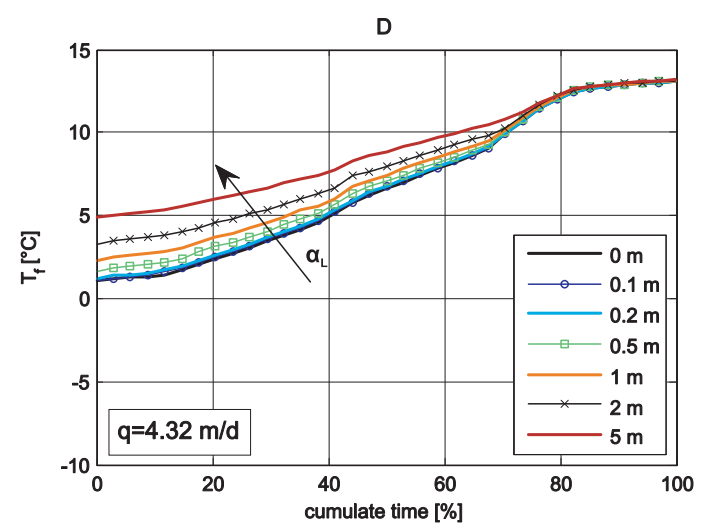
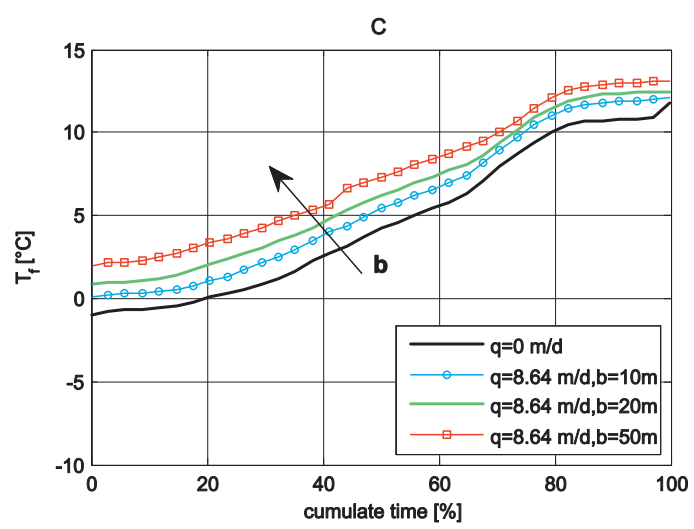
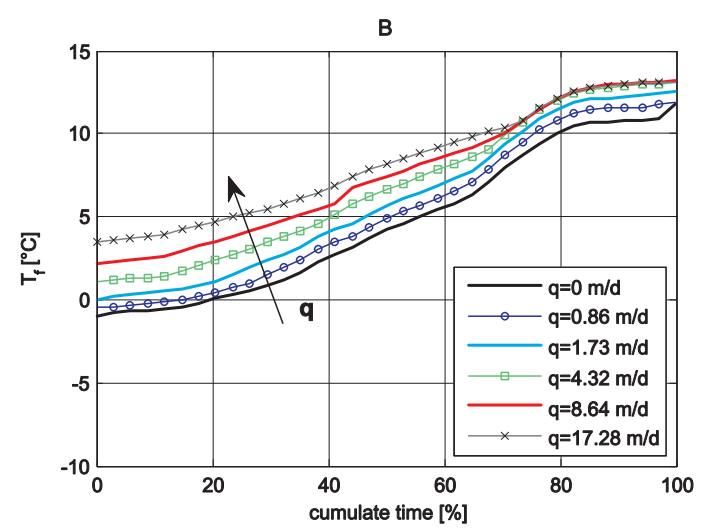
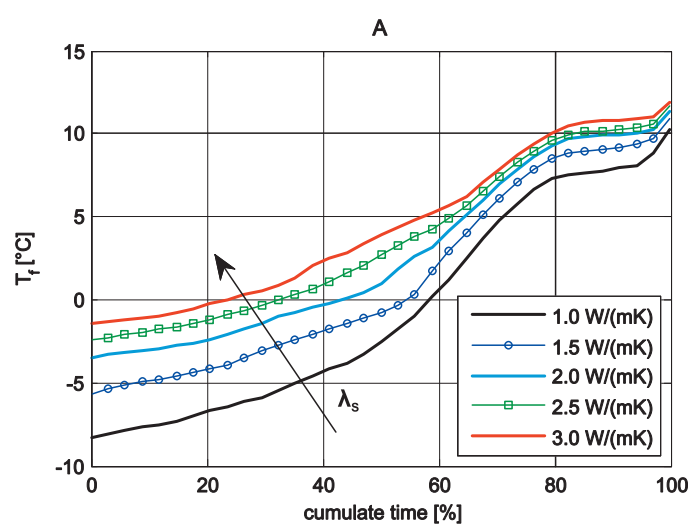


Fig.6

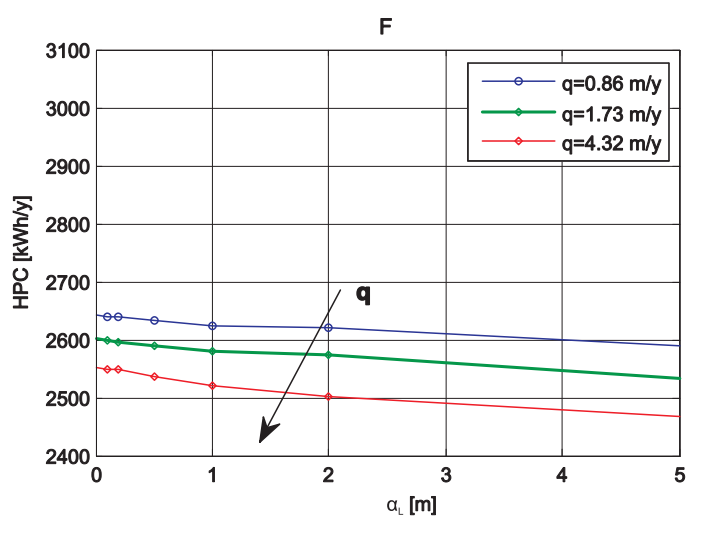
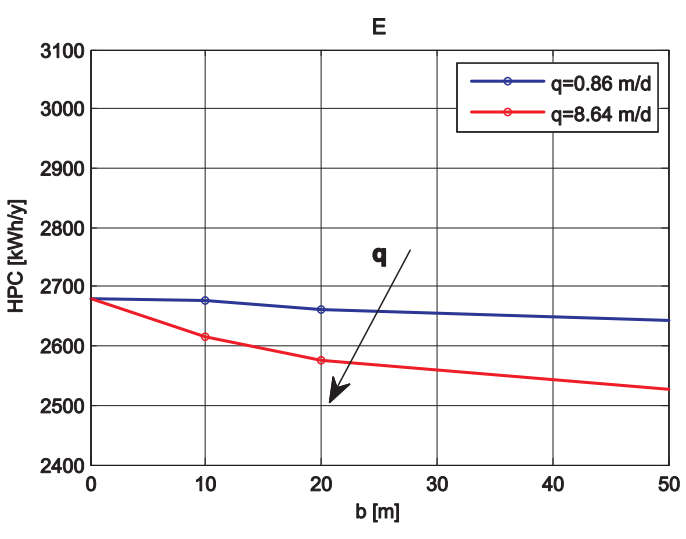
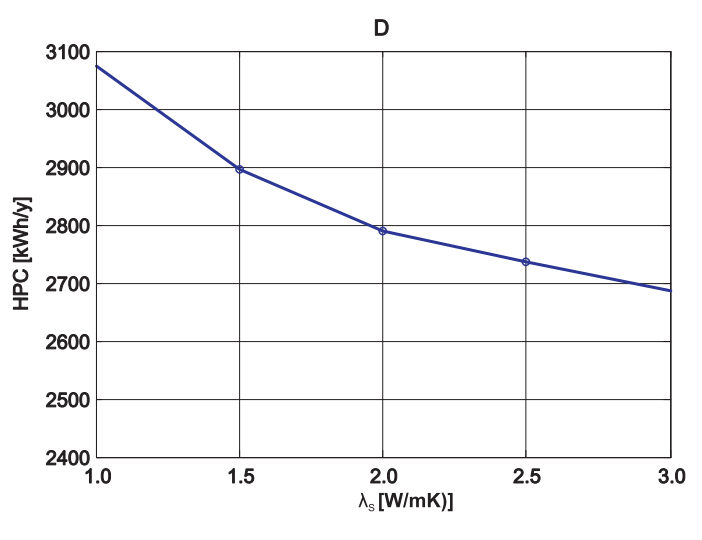
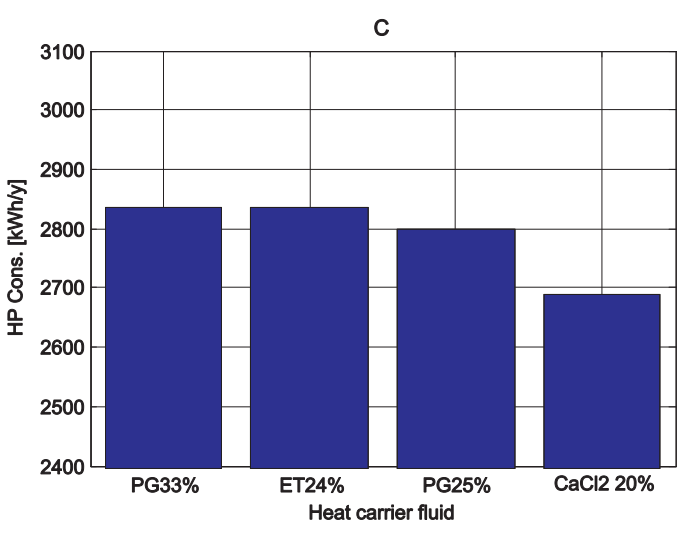
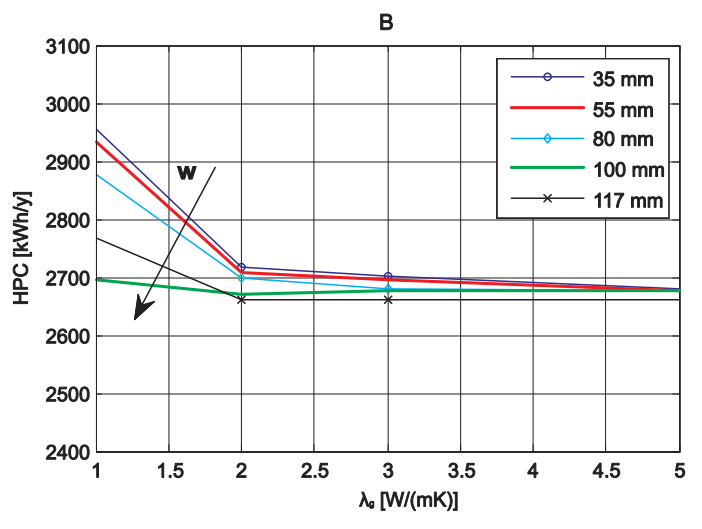
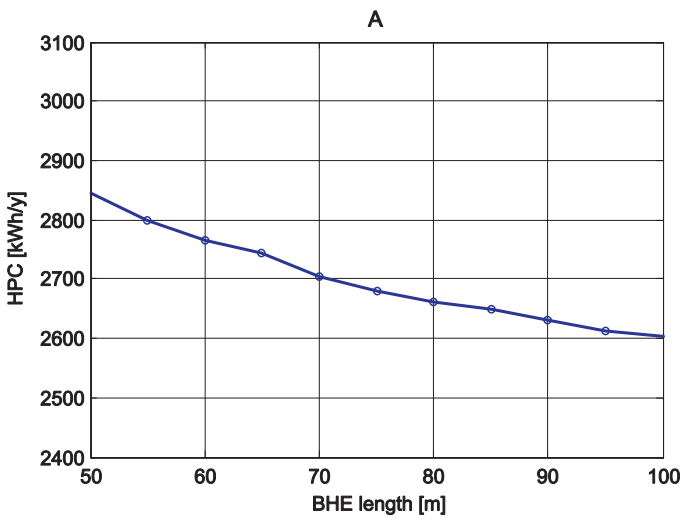


Fig.7

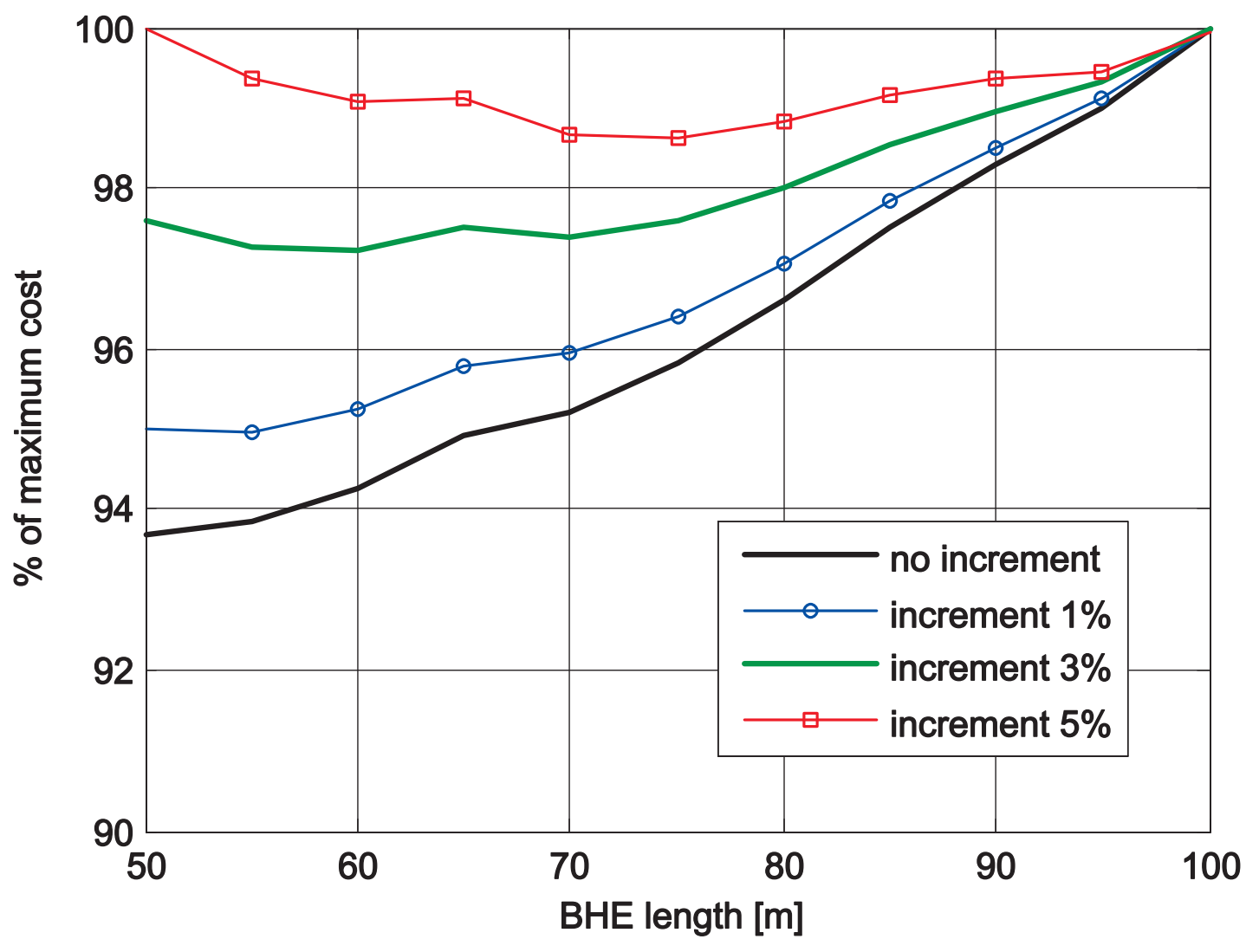


Fig.8

